New Journal of Physics
The open access journal for physics

A numerical study of the Navier–Stokes transport coefficients for two-dimensional granular hydrodynamics

Lidia Almazán[1,5], José A Carrillo[2], Clara Salueña[3], Vicente Garzó[4] and Thorsten Pöschel[1]

[1] Institute for Multiscale Simulation, Universität Erlangen-Nürnberg, D-91052 Erlangen, Germany
[2] Department of Mathematics, Imperial College London, London SW7 2AZ, UK
[3] Departament d'Enginyeria Mecànica, Universitat Rovira i Virgili, E-43007 Tarragona, Spain
[4] Departamento de Física, Universidad de Extremadura, E-06071 Badajoz, Spain
E-mail: lidia.t.almazan@cbi.uni-erlangen.de

New Journal of Physics **15** (2013) 043044 (25pp)
Received 28 November 2012
Published 25 April 2013
Online at http://www.njp.org/
doi:10.1088/1367-2630/15/4/043044

Abstract. A numerical study that aims to analyze the thermal mechanisms of unsteady, supersonic granular flow by means of hydrodynamic simulations of the Navier–Stokes granular equation is reported in this paper. For this purpose, a paradigmatic problem in granular dynamics such as the Faraday instability is selected. Two different approaches for the Navier–Stokes transport coefficients for granular materials are considered, namely the traditional Jenkins–Richman theory for moderately dense quasi-elastic grains and the improved Garzó–Dufty–Lutsko theory for arbitrary inelasticity, which we also present here. Both the solutions are compared with event-driven simulations of the same system under the same conditions, by analyzing the density, temperature and velocity field. Important differences are found between the two approaches, leading to interesting implications. In particular, the heat transfer

[5] Author to whom any correspondence should be addressed.

Content from this work may be used under the terms of the Creative Commons Attribution 3.0 licence. Any further distribution of this work must maintain attribution to the author(s) and the title of the work, journal citation and DOI.

© IOP Publishing Ltd and Deutsche Physikalische Gesellschaft

mechanism coupled to the density gradient, which is a distinctive feature of inelastic granular gases, is responsible for a major discrepancy in the temperature field and hence in the diffusion mechanisms.

Contents

1. Introduction

The hydrodynamics of granular materials is far from being well understood. The first difficulty comes from the kinetic theory level, where the far-from-equilibrium nature of the problem leads to both conceptual and technical limitations. Many contributions, starting from the 1980s [1, 2], have helped to develop a well-established hydrodynamic theory of granular gases, including mixtures and polydisperse materials. However, the application to other types of granular materials is still uncertain.

In academia as well as in industry, one would like to have a good theory for a variety of granular flow problems under different conditions. In the process of going from theory to real applications, one must resort to a good choice of transport coefficients to ensure an appropriate modeling of the system. The Navier–Stokes transport coefficients have been obtained for dilute and semi-dilute granular gases for selected problems within the framework of kinetic theory. However, their validity cannot be guaranteed beyond the conditions for which they were derived and as we enter the realm of moderately dense materials, where basic assumptions such as molecular chaos are not fulfilled. On the other hand, a purely empirical approach, such as the one used for regular liquids and where one measures the transport coefficients, to use them later in the Navier–Stokes equations, does not apply to granular hydrodynamics. The reason is that the properties of the flow depend strongly and nonlinearly on conditions such as the preparation of the system, flow rate and phenomena such as dilatancy; plus the fact that, in laboratory measurements, effects due to the surface properties of particles, wall roughness, the coupling with the interstitial fluid, etc are generally important. From the theoretical point of view, the treatment of granular materials by means of the available statistical–mechanics techniques faces inherent difficulties brought out by the dissipative character of real grain interactions, which is responsible for microscopic irreversibility, lack of scale separation, mesoscopic nature of the flow and strong nonlinearities in the governing equations.

One of the first attempts to determine the Navier–Stokes transport coefficients from the revised Enskog theory was made by Jenkins and Richman (JR) [1, 2]. However, the technical difficulties of the analysis entailed approximations that limited their accuracy. In particular, given that their analysis is restricted to nearly elastic systems, the inelasticity of collisions only influences the energy balance equation by a sink term, and so the expressions of the Navier–Stokes transport coefficients are the same as those obtained for elastic collisions. The JR approach has been numerically validated by molecular dynamics (MD) simulations in [3] and in experiments such as granular flow past an obstacle [4] and vertically oscillated granular layers [5–9]. The choice of vibrated granular material as a test case for hydrodynamic theories comes from being one of the simplest experiments in which all different regimes of the granular flow are present while leading to interesting standing-wave pattern formation and dynamics [10, 11], clustering [12, 13] and phase transitions [14–16].

One of the problems which has been repeatedly revisited as an interesting example of granular collective behavior is the granular Faraday instability. Similarly as in that described by Faraday for regular liquids [17], a vibrated granular layer develops characteristic patterns of stripes, hexagons and squares for certain intervals of frequencies and amplitudes of oscillation [11]. Experimentally and by means of particle simulations, the analogy to vibrated granular materials and regular fluids has been clearly shown. In two dimensions, at a certain stage of the motion the Faraday waves appear as shown in figure 7, whereas the time evolution of the periodic pattern, with twice the periodicity as that of the driving oscillation, can be seen in figure 3.

However, in many applications the dynamics of granular flow is supersonic, in a regime where the typical velocity of the flow is often many times or even orders of magnitude larger than the thermal velocity. To clarify concepts, the latter is proportional to the square root of the fluctuational part of the kinetic energy (which gives rise to the so-called granular temperature). More precisely, the vibrational regimes which are often imposed in real applications in order to mobilize granular material lead to an interplay of alternating diffusion and inertial regimes, giving rise to a rich although extremely complex dynamics, which we will analyze in detail here.

Beyond the weak dissipation limit, however, it is expected that the functional form of the Navier–Stokes transport coefficients for a granular gas differ from their corresponding elastic counterparts. Thus, in subsequent works Garzó and Dufty [18], and Lutsko (GDL) [19], based on the application of the Chapman–Enskog method [20] to the Enskog equation, do not impose any constraints at the level of collisional dissipation and take into account the (complete) nonlinear dependence of the Navier–Stokes transport coefficients on the coefficient of restitution α. In particular and in contrast to the JR results [1, 2], the heat flux has a contribution proportional to the density gradient which defines a new transport coefficient μ, which is not present in the elastic case. On the other hand, as for ordinary fluids [20], the Navier–Stokes transport coefficients are given in terms of the solutions of a set of coupled linear integral equations that are approximately solved by considering the leading terms in a Sonine polynomial expansion. In spite of this approximation, the corresponding forms for the transport coefficients compare well with computer simulations [21–23], even for quite strong inelasticity.

In a previous paper [7], we studied computationally the Faraday instability in vibrated granular discs, comparing the output from particle and Navier–Stokes hydrodynamic simulations in detail: the onset of the instability, the characteristic wavelength and the pattern itself by studying the density, temperature and velocity fields. This served to validate a

Navier–Stokes code for granular material based on a weighted essentially non-oscillatory (WENO) approach [24], which is capable of capturing the features of the highly supersonic flow generated by the impact of a piston. For this purpose, we used the JR expressions [1, 2] for the Navier–Stokes transport coefficients, valid for *elastic* hard spheres at moderate densities. The conclusion of the study was that the JR results showed qualitative and quantitative agreement with those from event-driven MD simulations, in a range of parameters which covered the entire bifurcation diagram of the Faraday instability at the coefficient of restitution $\alpha = 0.75$.

As already mentioned, the JR approach, however, fails in describing the heat flux accurately, since the transport coefficient μ coupled to the density gradient vanishes in the latter approach. The presence of this new term in the heat flux is crucial to explain, for instance, the dependence of the granular temperature on height in MD simulations in dilute vibrated systems with gradients only in the vertical direction [25–27]. Apart from that, a value of the coefficient of restitution of 0.75 justifies the use of correct forms of the Navier–Stokes transport coefficients proposed in the GDL approach [18, 19] which include the effect of dissipation on momentum and heat transport.

In the present paper, we follow a similar approach to that in [7] in order to study numerically the thermal mechanisms that an oscillating boundary imposes on granular material under gravity. That is, we will use the expressions of the Navier–Stokes transport coefficients derived in [18, 19] to compare the performance of the granular Navier–Stokes hydrodynamics with respect to particle simulations. We will also analyze the differences between the results provided by the JR approach [1, 2] and those from the current approximation [18, 19] to the Navier–Stokes transport coefficients.

The outline of the paper is as follows. In section 2, we will review the Navier–Stokes theory, introducing the GDL kinetic coefficients for dilute and moderately dense two-dimensional (2D) granular gases, opposed to the JR kinetic coefficients which are only valid for vanishing inelasticity. We will also explain briefly how to treat numerically the Navier–Stokes equations, while section 3 will be devoted to the results obtained with JR and GDL and their comparison with MD simulations. These will lead to interesting implications, which will be discussed in more detail in the conclusions.

2. The Navier–Stokes hydrodynamic theory of granular gases

We consider a granular fluid composed of smooth inelastic hard discs of mass m and diameter σ. Collisions are characterized by a (constant) coefficient of normal restitution $0 < \alpha \leqslant 1$. In a kinetic theory description, the relevant information on the system is contained in the one-particle velocity distribution function. At *moderate* densities and assuming molecular chaos, the velocity distribution function obeys the (inelastic) Enskog kinetic equation [28, 29]. Starting from this kinetic theory, one can easily obtain the (macroscopic) Navier–Stokes hydrodynamic equations for the number density $n(\vec{r}, t)$, the flow velocity $\vec{u}(\vec{r}, t)$ and the local temperature $T(\vec{r}, t)$ [30]. In the case of 2D granular gases, the balance equations read

$$\frac{\partial n}{\partial t} + \vec{\nabla} \cdot (n\vec{u}) = 0, \tag{1}$$

$$\rho \left(\frac{\partial \vec{u}}{\partial t} + \vec{u} \cdot \vec{\nabla} \vec{u} \right) = -\vec{\nabla} \cdot \hat{P} + n\vec{F} \tag{2}$$

and

$$n\left(\frac{\partial T}{\partial t}+\vec{u}\cdot\vec{\nabla}T\right)=-\nabla\cdot\vec{q}-\hat{P}:\vec{\nabla}\vec{u}-\zeta nT. \tag{3}$$

In the above equations, $\rho = mn$ is the mass density, $\vec{F}$ is the external force acting on the system, $\hat{P}$ is the pressure tensor, $\vec{q}$ is the heat flux and ζ is the cooling rate due to the energy dissipated in collisions. It is worthwhile to note that the macroscopic equations given in equations (1)–(3) differ from their counterparts for elastic fluids only via the appearance of the cooling rate ζ on the right-hand side of equation (3). On the other hand, the corresponding transport coefficients defining the momentum and heat fluxes must depend, in general, on the coefficient of restitution α.

As it happens for elastic fluids, the usefulness of the balance equations (1)–(3) is limited unless the fluxes and the cooling rate are specified in terms of the hydrodynamic fields and their spatial gradients. To first order in the spatial gradients, the Navier–Stokes constitutive equations provide a link between the exact balance equations and a closed set of equations for the hydrodynamic fields. The constitutive relation of the pressure tensor P_{ij} is

$$P_{ij}=p\delta_{ij}-\eta(\partial_j u_i+\partial_i u_j-\delta_{ij}\vec{\nabla}\cdot\vec{u})-\gamma\delta_{ij}\vec{\nabla}\cdot\vec{u}, \tag{4}$$

where p is the hydrostatic pressure, η is the shear viscosity and γ is the bulk viscosity. The constitutive equation for the heat flux is

$$\vec{q}=-\kappa\vec{\nabla}T-\mu\vec{\nabla}n, \tag{5}$$

where κ is the coefficient of thermal conductivity and μ is a new coefficient which does not have an analogue for a gas of elastic particles. Finally, to first order in gradients, the cooling rate ζ can be written as [28]

$$\zeta=\zeta_0+\zeta_1\nabla\cdot\vec{u}. \tag{6}$$

It is important to remark that the derivation of the Navier–Stokes order transport coefficients does not limit *in principle* their application to weak inelasticity. The Navier–Stokes hydrodynamic equations themselves may or may not be limited with respect to inelasticity, depending on the particular states considered. In particular, the derivation of these equations by means of the Chapman–Enskog method assumes that the spatial variations of the hydrodynamic fields n, $\vec{u}$ and T are small on the scale of the mean free path. In the case of ordinary fluids, the strength of the gradients can be controlled by the initial or boundary conditions. However, the problem is more complicated for granular fluids since in some cases (e.g. steady states such as the simple shear flow [31, 32]) there is an intrinsic relation between dissipation and some hydrodynamic gradient and so, the two cannot be chosen independently. Consequently, there are examples for which the Navier–Stokes approximation is never valid or is restricted to the quasielastic limit. On the other hand, the transport coefficients characterizing the Navier–Stokes order hydrodynamic equations are well-defined functions of α, regardless of the applicability of those equations.

As stated in the introduction, the evaluation of the explicit forms of the hydrostatic pressure p, the Navier–Stokes transport coefficients η, γ, κ and μ and the coefficients ζ_0 and ζ_1 requires us to solve the corresponding Enskog equation. However, due to the mathematical complexity of this kinetic equation, only approximate results for the above coefficients can be obtained. Here, we consider two independent approaches for hard discs that were proposed by Jenkins

and Richman [2] and Garzó and Dufty [18] and Lutsko [19]. Let us consider each method separately.

2.1. The Jenkins–Richman results

The results derived by Jenkins and Richman [1, 2] are obtained by solving the Enskog equation for spheres [1] and discs [2] by means of Grad's method [33]. The idea behind Grad's moment method is to expand the velocity distribution function in a complete set of orthogonal polynomials (generalized Hermite polynomials), the coefficients being the corresponding velocity moments. Next, the expansion is truncated after a certain order k. When this truncated expansion is substituted into the hierarchy of moment equations up to order k, one gets a closed set of coupled equations. In the case of a 2D system, the eight retained moments are the hydrodynamic fields (n, $\vec{u}$ and T) plus the irreversible momentum and heat fluxes ($P_{ij} - p\delta_{ij}$ and $\vec{q}$).

Although the application of Grad's method to the Enskog equation is not restricted to nearly elastic particles, the results derived by Jenkins and Richman [2] neglect the cooling effects on temperature due to the cooling rate in the expressions of the transport coefficients (see, for instance, equations (70), (89), (98), (99) and (100) of [2] when the discs are smooth). Given that this assumption can be considered acceptable only for nearly elastic systems, Jenkins and Richmanf [2] conclude that their theory holds only in the quasielastic limit ($\alpha \to 1$).

The explicit forms of the hydrostatic pressure, the Navier–Stokes transport coefficients and the cooling rate in the JR theory are given by

$$p_{\mathrm{JR}} = \frac{4}{\pi\sigma^2}\phi T[1+(1+\alpha)G(\phi)], \tag{7}$$

$$\eta_{\mathrm{JR}} = \frac{\phi}{2\sigma}\sqrt{\frac{mT}{\pi}}\left[\frac{1}{G(\phi)}+2+\left(1+\frac{8}{\pi}\right)G(\phi)\right], \tag{8}$$

$$\gamma_{\mathrm{JR}} = \frac{8}{\pi\sigma}\phi G(\phi)\sqrt{\frac{mT}{\pi}}, \tag{9}$$

$$\kappa_{\mathrm{JR}} = \frac{2\phi}{\sigma}\sqrt{\frac{T}{\pi m}}\left[\frac{1}{G(\phi)}+3+\left(\frac{9}{4}+\frac{4}{\pi}\right)G(\phi)\right], \tag{10}$$

$$\mu_{\mathrm{JR}} = 0,$$

$$\zeta_{0,\mathrm{JR}} = \frac{4}{\sigma}(1-\alpha^2)\sqrt{\frac{T}{\pi m}}G(\phi), \tag{11}$$

$$\zeta_{1,\mathrm{JR}} = 0.$$

In the above equations, $\phi = n\pi\sigma^2/4$ is the (dimensionless) volume fraction occupied by the granular discs, also called packing fraction, $G(\phi) = \phi\chi(\phi)$, and $\chi(\phi)$ is the pair correlation function.

Because of the assumption of near elastic particles in the JR theory, equations (7)–(11) show clearly that the coefficient of restitution α enters only in the equation of state (7) and in the expression (11) for the zeroth-order cooling rate ζ_0. At this level of approximation, the

expressions of the Navier–Stokes transport coefficients $\eta_{\rm JR}$, $\gamma_{\rm JR}$ and $\kappa_{\rm JR}$ are the same as those given by the Enskog equation for elastic discs [34].

In order to get the dependence of the transport coefficients and the cooling rate in both JR and GDL approaches, one has to chose an approximate form for the pair correlation function $\chi(\phi)$. In this paper, we have chosen the forms proposed by Torquato [35]

$$\chi(\phi) = \begin{cases} \dfrac{1-\frac{7}{16}\phi}{(1-\phi)^2} & \text{for } 0 \leqslant \phi < \phi_{\rm f}, \\ \dfrac{1-\frac{7}{16}\phi_{\rm f}}{(1-\phi_{\rm f})^2}\dfrac{\phi_{\rm c}-\phi_{\rm f}}{\phi_{\rm c}-\phi} & \text{for } \phi_{\rm f} \leqslant \phi \leqslant \phi_{\rm c} \end{cases} \tag{12}$$

which go through the freezing point $\phi_{\rm f} = 0.69$ and approach the random close packing fraction, $\phi_{\rm c} = 0.82$ with reasonable accuracy.

2.2. *The Garzó–Dufty–Lutsko results*

The dependence of the Navier–Stokes transport coefficients on the coefficient of restitution was first obtained by Garzó and Dufty [18] for hard spheres ($d = 3$) by solving the Enskog equation from the Chapman–Enskog method [20]. These results were then extended to an arbitrary number of dimensions by Lutsko [19]. Here, we refer to the above theories as the GDL theory. The Chapman–Enskog method [20] is a procedure to construct an approximate perturbative solution to the Enskog equation in powers of the spatial gradients. As stated in the introduction, the GDL theory considers situations where the spatial gradients are sufficiently small and *independent* of the coefficient of restitution α. As a consequence, the corresponding forms of the Navier–Stokes transport coefficients are not limited *a priori* to weak inelasticity since they incorporate the complete nonlinear dependence on α. This is the main difference with respect to the JR approach.

On the other hand, as to elastic collisions [20], the Navier–Stokes transport coefficients in the Chapman–Enskog method cannot be *exactly* determined since they are defined in terms of the solutions of a set of coupled linear integral equations. It is useful to represent these solutions as an expansion in a complete set of polynomials (Sonine polynomials) and generate approximations by truncating the expansion. In practice, the leading terms in these expansions provide an accurate description over the full range of dissipation and density since, in general, they yield good agreement with Monte Carlo simulations, except for the heat flux transport coefficients at high dissipation [21, 22]. Motivated by this disagreement, a modified version of the first Sonine approximation has recently been proposed [23, 36]. The modified Sonine approximation replaces the Gaussian weight function (used in the standard Sonine method) by the homogeneous cooling state distribution. This new method significantly improves the α-dependence of κ and μ since it partially eliminates the discrepancies between simulation and theory for quite a strong dissipation (see, for instance, figures 1–3 of [23]).

The results obtained in the GDL approach for the equation of state and the Navier–Stokes transport coefficients for hard discs ($d = 2$) are

$$p_{\rm GDL} = p_{\rm JR} = \frac{4}{\pi\sigma^2}\phi T[1+(1+\alpha)G(\phi)], \tag{13}$$

$$\gamma_{\rm GDL} = \frac{4}{\pi\sigma}\phi G(\phi)\sqrt{\frac{mT}{\pi}}(1+\alpha)\left(1-\frac{c}{32}\right), \tag{14}$$

$$\eta_{\rm GDL}=\frac{\sqrt{mT/\pi}}{2\sigma}\frac{\left[1-\frac{1}{4}(1+\alpha)(1-3\alpha)G(\phi)\right]\left[1+\frac{1}{2}G(\phi)(1+\alpha)\right]}{\nu_\eta^*-\frac{1}{2}\zeta_0^*}+\frac{1}{2}\gamma_{\rm GDL}, \tag{15}$$

$$\kappa_{\rm GDL}=\frac{2}{\sigma}\sqrt{\frac{T}{\pi m}}\left\{\left[1+\frac{3}{4}G(\phi)(1+\alpha)\right]\kappa_k^*+\frac{2}{\pi}\phi G(\phi)(1+\alpha)\left(1+\frac{7c}{32}\right)\right\}, \tag{16}$$

$$\mu_{\rm GDL}=\frac{T\sigma}{\phi}\sqrt{\frac{\pi T}{m}}\left[1+\frac{3}{4}G(\phi)(1+\alpha)\right]\mu_k^*, \tag{17}$$

where the (reduced) kinetic contributions κ_k^* and μ_k^* are

$$\kappa_k^*=\frac{1+c+\frac{3}{8}G(\phi)(1+\alpha)^2\left[2\alpha-1+\frac{c}{2}(1+\alpha)\right]}{2(\nu_\kappa^*-2\zeta_0^*)}, \tag{18}$$

$$\mu_k^*=\frac{\zeta_0^*\kappa_k^*(1+\phi\partial_\phi\ln\chi)+\frac{c}{4}+\frac{3}{8}G(\phi)(1+\alpha)(1+\frac{1}{2}\phi\partial_\phi\ln\chi)\left[\alpha(\alpha-1)+\frac{c}{12}(14-3\alpha+3\alpha^2)\right]}{2\nu_\kappa^*-3\zeta_0^*}. \tag{19}$$

In equations (15)–(19), we have introduced the quantities [36]

$$\zeta_0^*=\frac{1}{2}\chi(\phi)(1-\alpha^2)\left(1+\frac{3c}{32}\right), \tag{20}$$

$$\nu_\eta^*=\frac{1}{8}\chi(\phi)(7-3\alpha)(1+\alpha)\left(1+\frac{7c}{32}\right), \tag{21}$$

$$\nu_\kappa^*=\frac{1}{4}\chi(\phi)(1+\alpha)\left[1+\frac{15}{4}(1-\alpha)+\frac{365-273\alpha}{128}c\right], \tag{22}$$

where

$$c(\alpha)=\frac{32(1-\alpha)(1-2\alpha^2)}{57-25\alpha+30\alpha^2(1-\alpha)} \tag{23}$$

is the fourth cumulant coefficient measuring the deviation of the homogeneous reference state from its Gaussian form. Also taking into account equation (12), we obtain the expression to be used in equation (19).

It is quite apparent that, except the equation of state (13), the expressions for the Navier–Stokes transport coefficients of the GDL results clearly differ from those obtained in the JR approach. In fact, equations (14)–(17) of the GDL theory reduce to equations (8)–(10), respectively, in the elastic limit ($\alpha=1$ and so $\zeta_0^*=c=0$). Note that the expressions derived by Lutsko [19] neglect in the expressions (21) and (22) of ν_η^* and ν_κ^*, respectively, the factors of c coming from the non-Gaussian corrections to the reference state. These extra factors will be accounted for in our numerical results since their effect on transport becomes non-negligible at small values of α. In figure 1 we show the ratio between the bulk viscosity, shear viscosity and thermal conductivity given by the GDL and JR approaches as a function of the coefficient of restitution α for different packing fractions ϕ. Note that the bulk viscosity ratio does not depend on ϕ. We also observe the order of magnitude of the new term in the heat flux due to the density gradient in the GDL theory with respect to the heat flux of the JR theory. The quantitative percentage of deviation of the transport coefficients with the GDL theory from the JR theory is

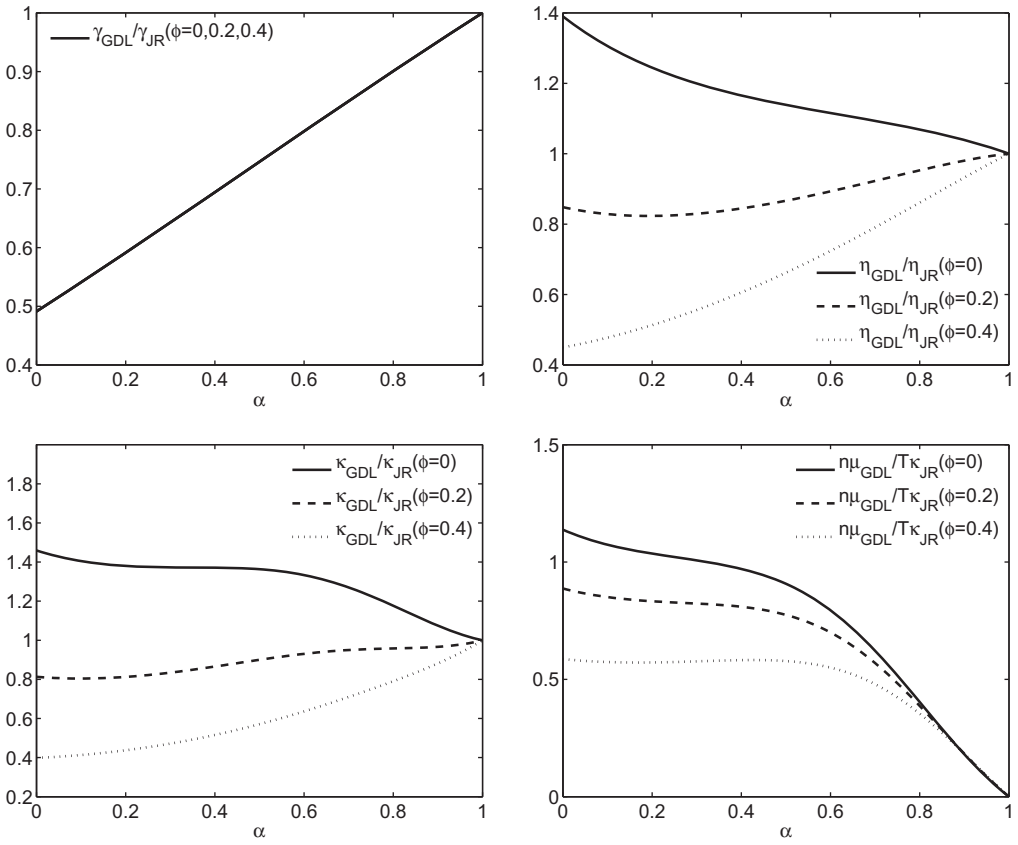

Figure 1. The bulk viscosity ratio $\gamma_{\rm GDL}/\gamma_{\rm JR}$ (top left), shear viscosity ratio $\eta_{\rm GDL}/\eta_{\rm JR}$ (top right), thermal conductivity ratio $\kappa_{\rm GDL}/\kappa_{\rm JR}$ (bottom left) and $n\mu_{\rm GDL}/T\kappa_{\rm JR}$ ratio (bottom right) as a function of the restitution coefficient α for three different values of the packing fraction ϕ: $\phi = 0$ (solid line), $\phi = 0.2$ (dashed line) and $\phi = 0.4$ (dotted line).

quite significant for $\alpha = 0.8$ and the different packing fractions ϕ used. We emphasize how the GDL term related to the density gradient in the heat flux becomes very important for $\alpha \leqslant 0.8$.

Finally, the contributions to the cooling rate are given by

$$\zeta_{0,\rm GDL} = \frac{4}{\sigma}(1-\alpha^2)\sqrt{\frac{T}{\pi m}}G(\phi)\left(1+\frac{3c}{32}\right), \tag{24}$$

$$\zeta_{1,\rm GDL} = \frac{3}{2}G(\phi)(1-\alpha^2)\left[\frac{3}{32}\frac{\frac{1}{8}\omega^* - c(1+\alpha)(\frac{1}{3}-\alpha)}{\nu_\zeta^* - \frac{3}{4}(1-\alpha^2)} - 1\right], \tag{25}$$

where

$$\nu_\zeta^* = -\frac{1+\alpha}{192}(30\alpha^3 - 30\alpha^2 + 153\alpha - 185), \tag{26}$$

$$\omega^* = (1+\alpha)\left[(1-\alpha^2)(5\alpha-1) - \frac{c}{12}(15\alpha^3 - 3\alpha^2 + 69\alpha - 41)\right]. \tag{27}$$

Equation (24) agrees with its corresponding counterpart in the JR theory, equation (11), when one neglects the non-Gaussian corrections to the reference state ($c = 0$). Note that ζ_1 vanishes in

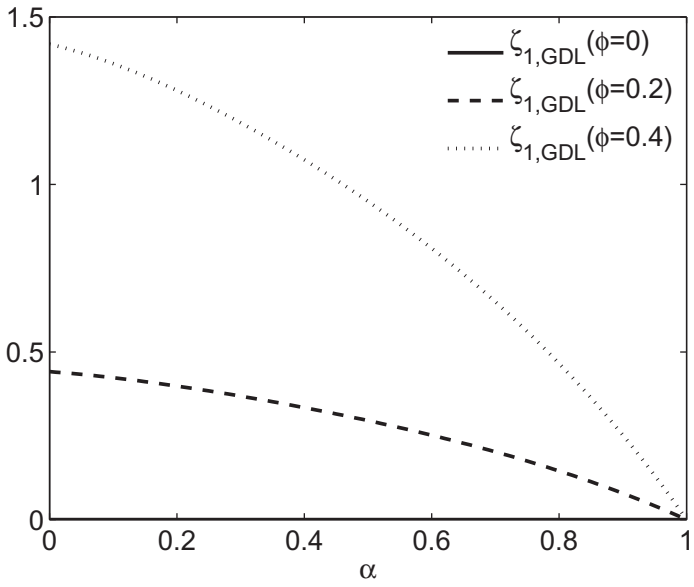

Figure 2. First-order correction of the cooling coefficient for GDL theory as a function of the coefficient of restitution α for three different values of the packing fraction ϕ: $\phi = 0$ (solid line), $\phi = 0.2$ (dashed line) and $\phi = 0.4$ (dotted line).

limits of elastic gases ($\alpha = 1$, arbitrary volume fraction ϕ) and of dilute inelastic gases ($\phi = 0$, arbitrary values of the coefficient of restitution α). In figure 2, we plot the α-dependence of $\zeta_{1,\mathrm{GDL}}$. We observe that the first-order contribution to the total cooling rate appears to be more significant as the gas becomes denser.

2.3. Numerical scheme for the hydrodynamic granular equations

The compressible Navier–Stokes-like equations for granular materials (1)–(3) are solved in conservation form for the convective terms; that is, we numerically solve the system for the density, the momentum and the total energy: $(n, n\vec{u}, W)$ where the total energy density W is given by

$$W = nT + \tfrac{1}{2}n|\vec{u}|^2. \tag{28}$$

This system can be rewritten as a system of nonlinear conservation laws with sources as in [7]. Local eigenvalues and both local left- and right-eigenvectors of the Jacobian matrices of the fluxes are explicitly computable (see the appendix of [7]). We only mention here that the characteristic speeds of the waves in the hyperbolic part of the equation can be written in terms of the speed of sound, given by

$$c_s^2 = \frac{\partial p}{\partial n} + \frac{p}{n^2}\frac{\partial p}{\partial \epsilon} \tag{29}$$

for a general equation of state where $p = p(n, \epsilon)$ with the enthalpy $\epsilon = T$ for a 2D system. See [7] for full details of the numerical scheme that is applied here to both the GDL and the JR Navier–Stokes hydrodynamic equations since they share the same structure. Let us briefly mention that Navier–Stokes terms are treated by simple centered high-order explicit in time finite difference approximations and considered as sources of the method of lines in the time

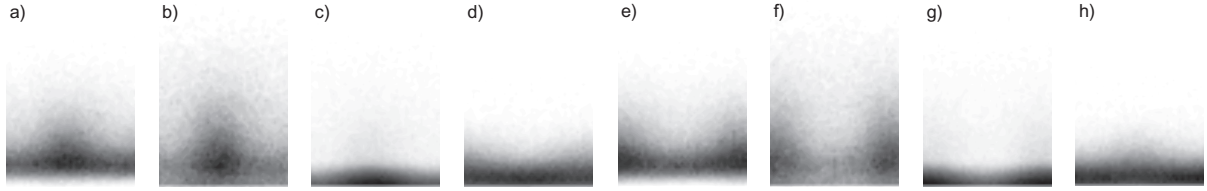

Figure 3. Density field obtained by phase- and space-averaging particle positions from the MD simulation. One single wavelength is shown along eight equidistant phases (a)–(h).

approximation. Meanwhile, the Euler (convective) terms are solved in local coordinates by a fifth-order explicit in time finite difference characteristic-wise WENO method in a uniform grid following [24, 37]. Thus, typical wave speeds and vectors, eigenvalues and eigenvectors of the purely hyperbolic part, are correctly resolved.

3. Results

We have applied the traditional MD approach to compare the results obtained from the Navier–Stokes hydrodynamic equations with the GDL kinetic coefficients, showing also those results provided by the previously used JR model as a reference. In all simulations, the frequency of the piston motion is $f = 3.75$ Hz and the amplitude is $A = 5.6$ particle diameters. The system size is tuned to fit three pattern wavelengths in the (horizontal) x-direction ($125\,\sigma$), which is periodic. In the (vertical) y-direction, the hydrodynamic simulations are constrained into a box of finite height of 60 diameters, whereas the MD system is not limited (particles reach the height of 60 diameters very rarely). The particles are 783 discs of diameter $\sigma = 1$ cm and mass $m = 1$ mg and $g = 9.81\,\mathrm{m\,s^{-2}}$ is the acceleration of gravity. The coefficient of restitution is $\alpha = 0.80$; however, a similar behavior is found regardless of the value of the coefficient of restitution between $\alpha = 0.60$ and 0.80. At $\alpha = 0.85$ and beyond instead, the pattern does not form in our system. Since JR and GDL will differ less and less, the differences will shrink at high values of α anyway. The interesting region is found at intermediate values of α, whereas the use of JR is clearly wrong at very low values of the coefficient of restitution. Therefore, we will show the results for $\alpha = 0.80$ as a representative case of what one will observe under the conditions of the Faraday instability.

The top and bottom walls in both hydrodynamic simulations are adiabatic and impenetrable. More precisely, the normal velocity is zero at the walls, the energy flux is zero and the tangential velocity remains unchanged. The simulation is carried over in the comoving frame of the wall, and thus the force per unit mass of the simulated system is $\vec{F} = -g(1 + A\sin(2\pi f t))\vec{j}$, with $\vec{j} = (0, 1)$.

See [7] for details of the averaging procedure applied to the MD sequence, here consisting of 1000 cycles, which leads to the averaged (2D) MD hydrodynamic fields for the density (packing fraction) (figure 3), linear momentum and thermal energy. From the latter, the temperature field is also obtained. These are compared with the corresponding ones generated by the two hydrodynamic simulations.

We disregard the transient originating from the initial condition until the pattern of the Faraday instability has fully developed and no changes are observed from period to period.

After this transient time, which takes about 50 periods of forcing, the system reveals a subharmonic periodic dynamics where the period is twice the period of the forcing f^{-1}. In this regime, we fix the reference time $t = 0$ and consider the evolution of the profiles of packing fraction, figure 4, scaled thermal energy, figure 5, scaled granular temperature, figure 6, and scaled kinetic energy, figure 10, using equation (28). The subfigures (a)–(h) correspond to the times $t = 0;\ 1/4f^{-1};\ 2/4f^{-1};\ \ldots;\ 7/4f^{-1}$. The corresponding position of the piston is $y = -A\sin 2\pi ft$. Despite the fact that the hydrodynamic fields are two-dimensional, we show one-dimensional profiles for a more detailed quantitative analysis. Thus, the profiles shown in figures 4–6 are taken at a representative location along the abscissa, where the amplitude of the Faraday pattern is developed. The evolution of these profiles over the period of excitation is also presented as supplementary online material [38], showing the profiles at many more intermediate times.

3.1. Density

First of all, we are going to discuss the behavior of the packing fraction (figure 4). Since the packing fraction is proportional to the number density $\phi = \pi\sigma^2 n/4$, we will use both terms indistinctly. As in subsequent figures, the abscissa represents the height, in diameters. On the ordinate we show here the packing fraction. The evolution is shown from left to right and then from top to bottom. Note that the integral of each curve is not the same for the hydrodynamics and the MD simulations since it corresponds just to a vertical cut at a position where the maximum height of the pattern is achieved. Total conservation of mass is maintained in all simulations with high accuracy, see [7] for more details.

At time $t = 0$, figure 4(a), the piston is going down through the equilibrium position. The height of the material at this location has already grown to a maximum, formed at the end of the previous cycle (g) and (h). Shortly after this time, the granular layer experiences the impact against the bottom wall and the propagation of a shock wave. Between (a) and (c), we see the dissolution of the peak. We observe that the GDL prediction is denser than the JR at a distance of 10 diameters from the plate. Just instants following frame (c), the layer becomes flat—so it does after frame (g), and the material floods to neighboring positions to create peaks where valleys previously existed. Shortly after (d), another impact with the plate takes place. From frame (d) to frame (g), we see the evolution of the density at a valley.

The MD sequence reveals that the maximum density 0.69 in the packing fraction is smaller than in both hydrodynamic simulations, reaching the value 0.78. This can be due to the irregularity of the MD pattern due to the elasticity of the system at $\alpha = 0.80$, which makes the location of any of the peaks of the MD sequence somewhat uncertain. We recall that the granular Navier–Stokes solver does not contain fluctuational—mesoscopic—contributions, while the local noise is enhanced by increasing the coefficient of restitution. That is why one needs a factor of 20 times more cycles to obtain smooth fields, as compared with the results at $\alpha = 0.75$, obtained in our previous study [7]. There the regularity was much more pronounced, and much better agreement was achieved.

The role of fluctuating hydrodynamics in granular gases has been an object of study for the last decade, since Van Noije *et al* [39], or more recently, Brey [40] and Costantini [41]. The essentially mesoscopic dynamics of the granular gas flow cannot be fully captured by means of macroscopic transport equations. This is easily emphasized, for instance, by the need to apply mesoscoping averaging to MD results, in order to compare particle and hydrodynamic simulations. Another related effect is the diffusion found at the level of the bifurcation threshold

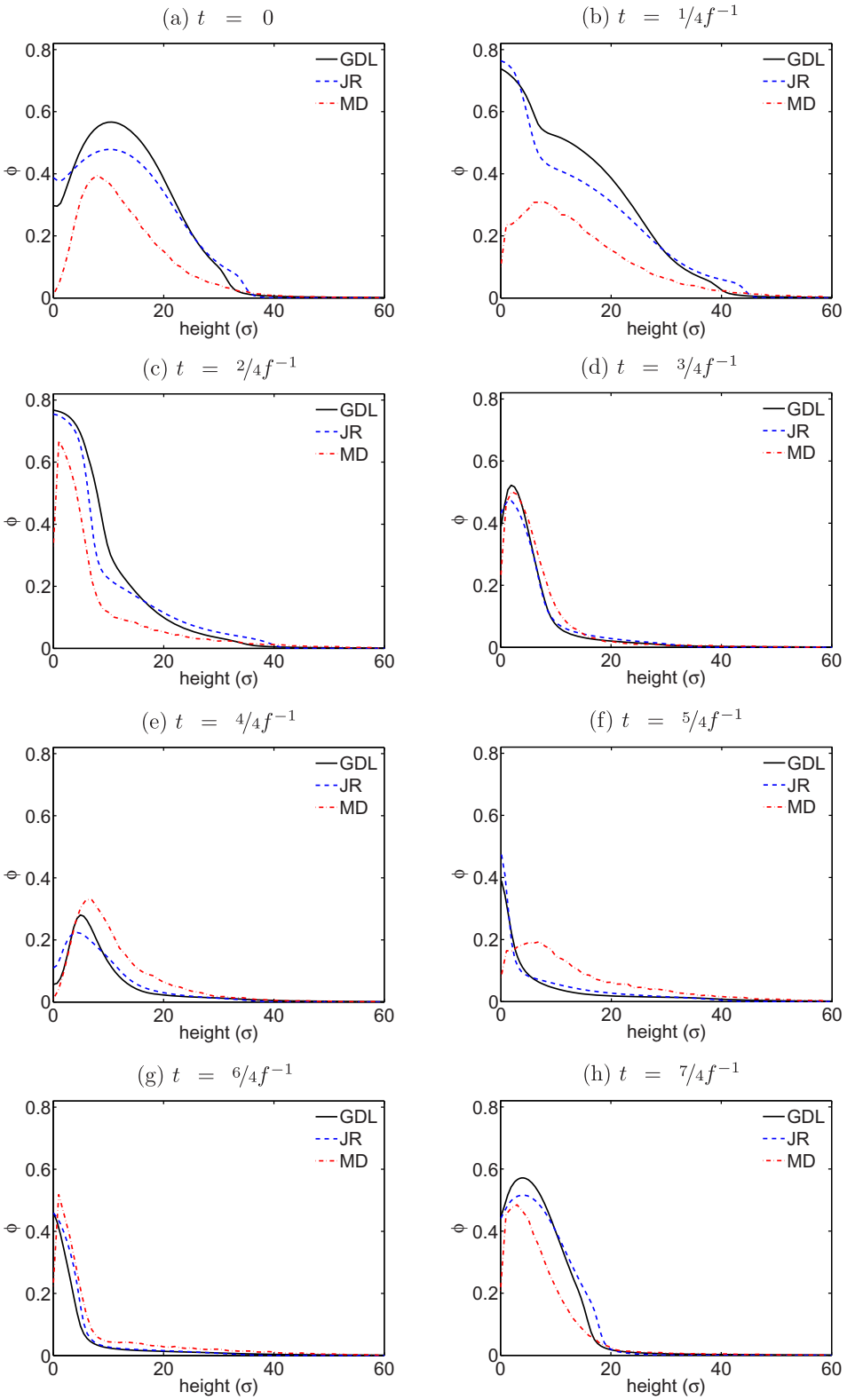

Figure 4. The profiles of the packing fraction (ϕ) as a function of height (in units of σ) at selected times over two oscillation periods. For time evolution of the profiles see [38].

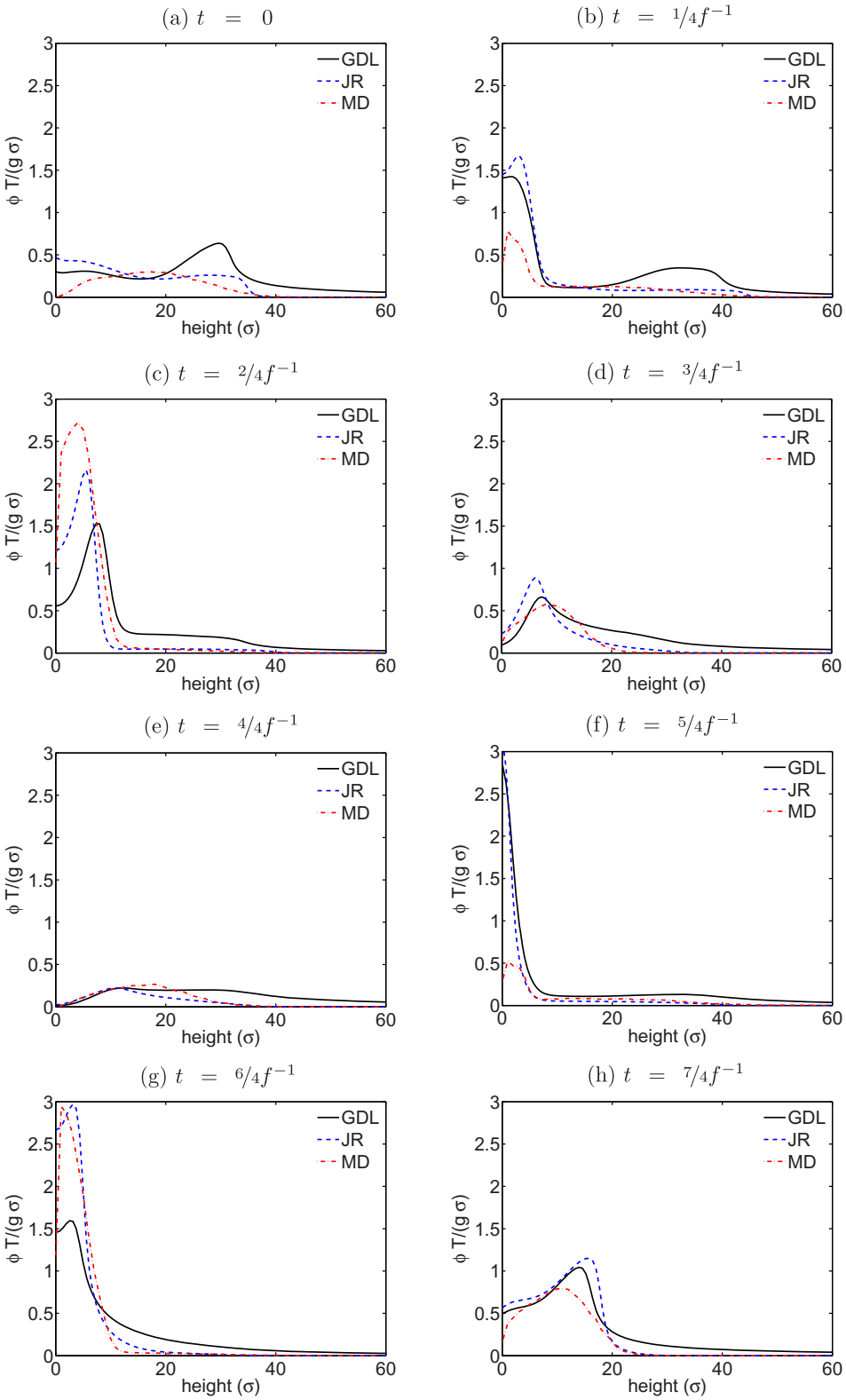

Figure 5. Scaled internal energy ($\phi T/(\sigma g)$) as a function of height (in units of σ) at selected times over two oscillation periods. For time evolution of the profiles see [38].

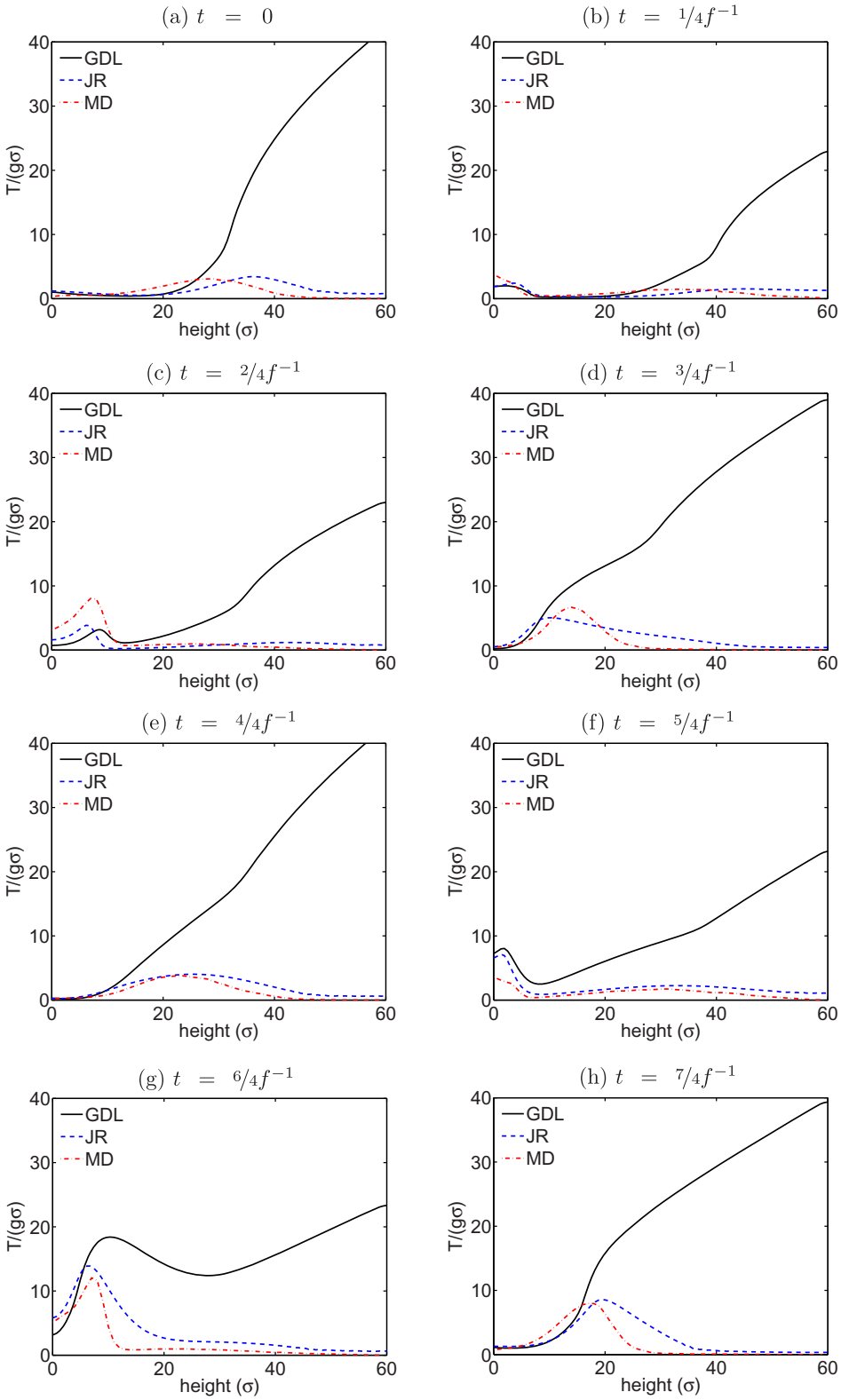

Figure 6. Profiles of the temperature $(T/(\sigma g))$ as a function of height (in units of σ) at selected times over two oscillation periods for the MD system and the JR and GDL solutions. For time evolution of the profiles see [38].

Figure 7. A snapshot of the MD simulation at the maximum opening of the gap ($t \approx 0.12\ f^{-1}$), showing the material stuck at the bottom, between the peaks and the plate, whereas there is a completely empty space below the valleys.

of the instability, as observed from MD simulations; the hydrodynamic simulations show instead a sharp inception of the instability at about $\Gamma = 2.0$, when one represents the wavelength of the Faraday pattern as a function of the reduced acceleration Γ of the plate [7]. We expect (minor) differences between the two models in the pattern wavelength; however, we did not perform the complete analysis of the bifurcation diagram in the case of the GDL model for the following reason. As a result of what we have explained above, at the threshold of the Faraday instability, the uncertainty in the wavelength as determined by the Fourier analysis of the density pattern is quite large [7]. The presence of noise turns the transition into a continuous phenomenon, which the hydrodynamic simulations without a source of fluctuations cannot exactly reproduce. As a consequence, both the JR and the GDL models will be providing somewhat different thresholds, none of which will be accounting for the true effect. Beyond the instability threshold, we do observe different wavelengths for the case analyzed: 5.6 diameters of amplitude of vibration, and reduced acceleration of 2.75. For these parameters, a system 500 wide shows 12 wavelengths in the JR simulation, whereas the GDL shows 13. The MD also shows 13. This implies that the GDL approach models better this feature as compared with JR, at least for the values of the parameters chosen.

While the GDL and JR profiles do not differ greatly, there are some differences: the GDL density is higher at the core of peaks and valleys, as compared to the JR prediction at equivalent times. Correspondingly, the packing fraction at the bottom plate is smaller in the GDL simulation, and so is the minimum density (0.054 versus the value of 0.112 obtained in the JR simulation). However, the minimum density in the averaged MD profile is still smaller: 0.004. Also, the impact with the plate occurs later as compared with both hydrodynamic simulations, the delay being about $0.16\,f^{-1}$. Therefore, we may argue that, in general, the accurate expressions of the GDL approximation for the Navier–Stokes transport coefficients do not greatly improve the density profile obtained with the elastic forms of the JR approach to match the MD results in this problem. A direct comparison of the time evolution of densities and velocity fields in full spacial resolution can be found in the supplementary material [38].

A zoom of the region of the MD system close to the plate during the airborne phase will show a few particles stuck to the base of the peaks and empty areas with no particles at all below the valleys (figure 7). As a consequence, the impact of the wall against the material happens at $t = 0.16\,f^{-1}$ (instead of $t = 0$). We want to remark that this piece of the system is not in the hydrodynamic regime at this moment, but in the Knudsen regime, and there is little hope that

any hydrodynamic model can reproduce this feature in full detail. However, the GDL approach to the Navier–Stokes equations improves the dynamics of the gap formed as compared with the JR approach in the sense that the minimum density at the bottom plate is reduced. On the other hand, the density gradients are higher in the GDL theory, a feature that is not observed in the MD profiles, which are smoother. The differences are basically due to the presence of the coefficient μ_{GDL} (equation (19) of the GDL model), which is absent ($\mu_{\mathrm{JR}} = 0$) in the elastic case (the JR approach).

3.2. Temperature and internal energy

In figure 5, we plot the scaled internal energy, $\phi T/(\sigma g)$, where g denotes the gravity acceleration. Here we see the evolution of the shock wave traveling across the granular layer. We can observe that the energy is smaller everywhere in the GDL system, except at intermediate and large heights. Remarkably, the energy of the GDL shock wave is lower than the JR after an impact with the wall; however, the remnants persist for long at larger heights. The MD profile indicates a higher energy at the bottom after an impact (c), as compared with both GDL and JR results, but especially with the latter. The GDL shock wave is very much damped. It also shows that the impact with the bottom wall occurs effectively later, as pointed out when discussing the density profiles. In addition, the MD profile shows that the energy vanishes more quickly than in the GDL solution. Let us examine then the temperature field.

The most striking difference between the GDL and JR solutions is the temperature field (figure 6). At large heights, the GDL temperature is one order of magnitude larger than the JR. Moreover, the GDL temperature gradient is positive at middle heights (it starts to grow), whereas there the JR, like the MD temperature gradient, is negative once the shock wave is dissipated. It is clear that the term $\mu\nabla n$ helps to sustain large temperature gradients in the system, transferring heat from the dense to the dilute regions at the top wall. This term is the genuine contribution of the inelastic nature of the granular gas to the transport coefficients, although we find no hint in the obtained MD profile that the temperature gradient should be positive instead of negative when ascending from the dense to the dilute region. As mentioned in the introduction, the presence of the coefficient μ in the heat flux is an *exact* result of the inelastic Enskog equation and the JR approximation fails in describing this new effect. In addition, the existence of this term in the heat flux has been already confirmed by computer simulation results [25].

However, one must recall that beyond 40 diameters in height the material gets more and more rarefied (figure 4) and goes from densities of the order of 1% in packing fraction at 40 diameters to about 0.1% at 60, as obtained from MD results. Therefore, one should find Knudsen layers when approaching a virtual top wall—in our MD simulations there is none, making our hydrodynamic simulations meaningless there. Note, on the other hand, that the temperature field T displayed in figure 6, when scaled with the mean free path as the relevant unit length, will be proportional to the quantity ϕT displayed in figure 5. In the latter, one can appreciate that the mismatch between JR and GDL is reduced, although it still persists. Also, by comparing the three figures (figures 4–6), we find that the growth of the temperature starts at intermediate heights, when the density is not especially small. For this reason, one can conclude that the growth of the temperature is a true result of the GDL approach and not a negligible product.

As the GDL temperature is higher than the JR temperature at the top, the GDL solution is more diffusive. Figure 8 shows the vertical component of the heat flux as a function of height, where this effect is shown: note the enhanced heat transport at intermediate heights, as compared

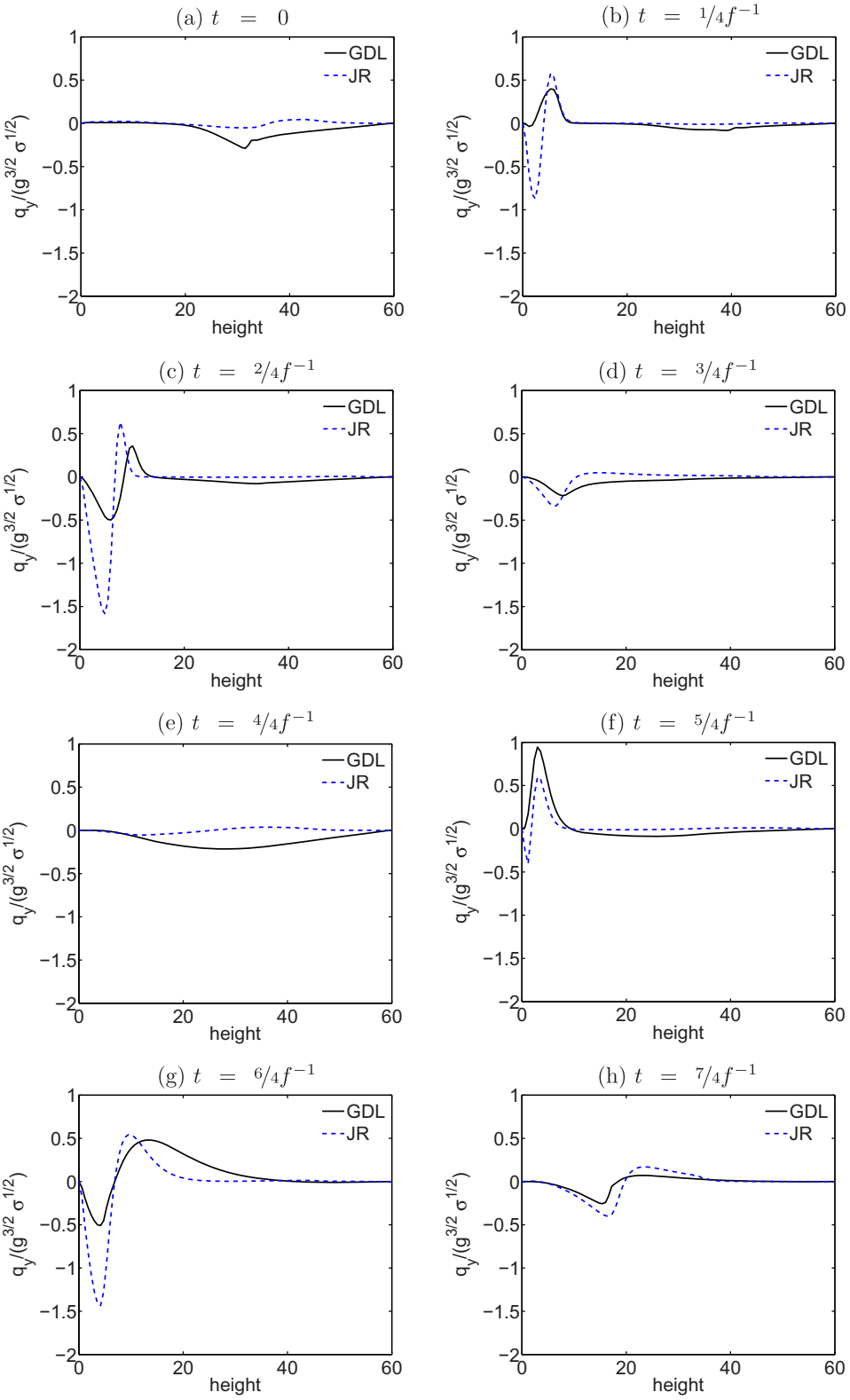

Figure 8. Vertical component of the (reduced) heat flux as a function of height (in units of σ) at selected times over two oscillation periods, for the JR and GDL simulations. For the time evolution of the profiles, see [38].

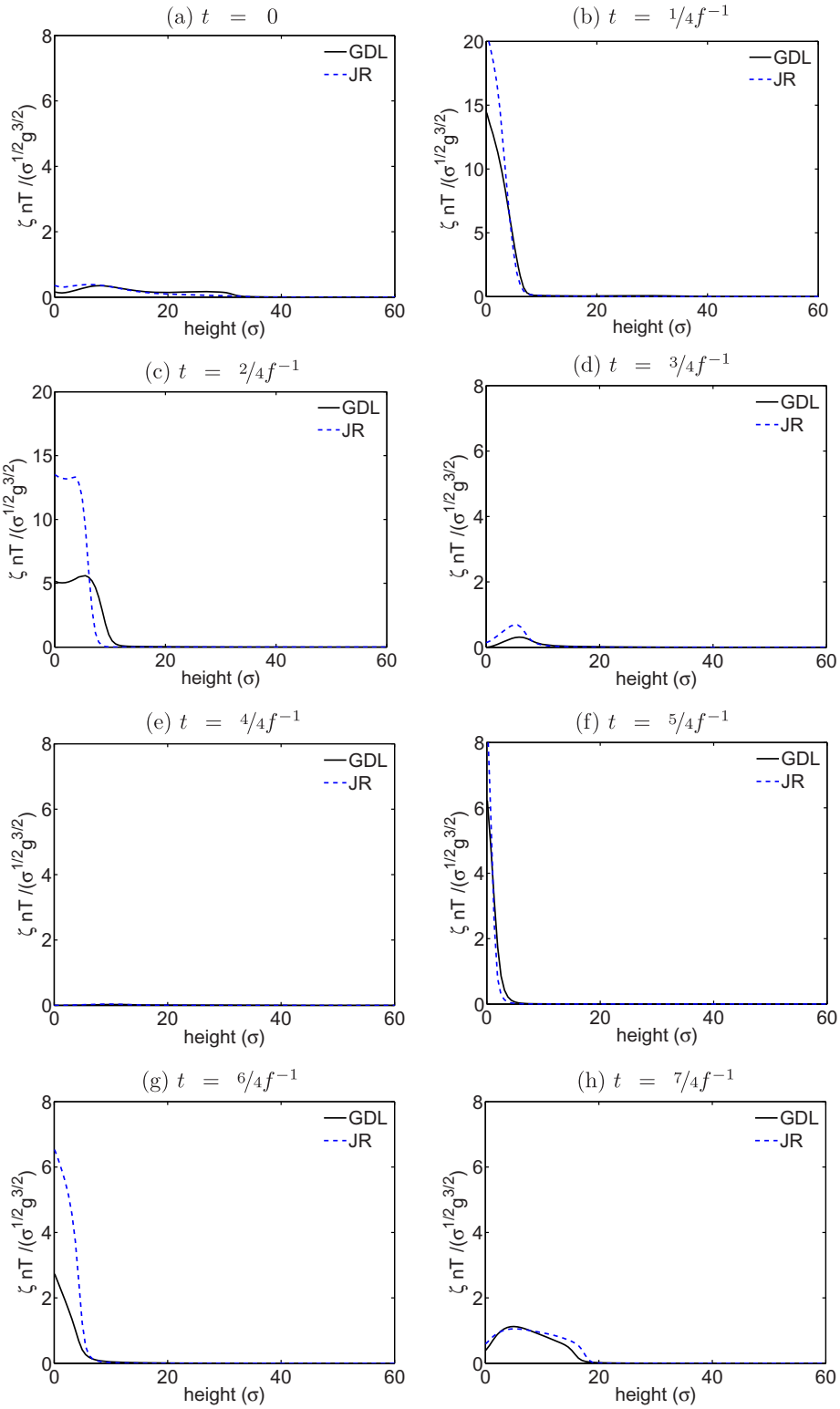

Figure 9. The profiles of the cooling term ζnT as a function of height (in units of σ), at selected times over two oscillation periods, for the JR and GDL simulations. Note the change in the vertical scale in subfigures (b) and (c). For time evolution of the profiles, see [38].

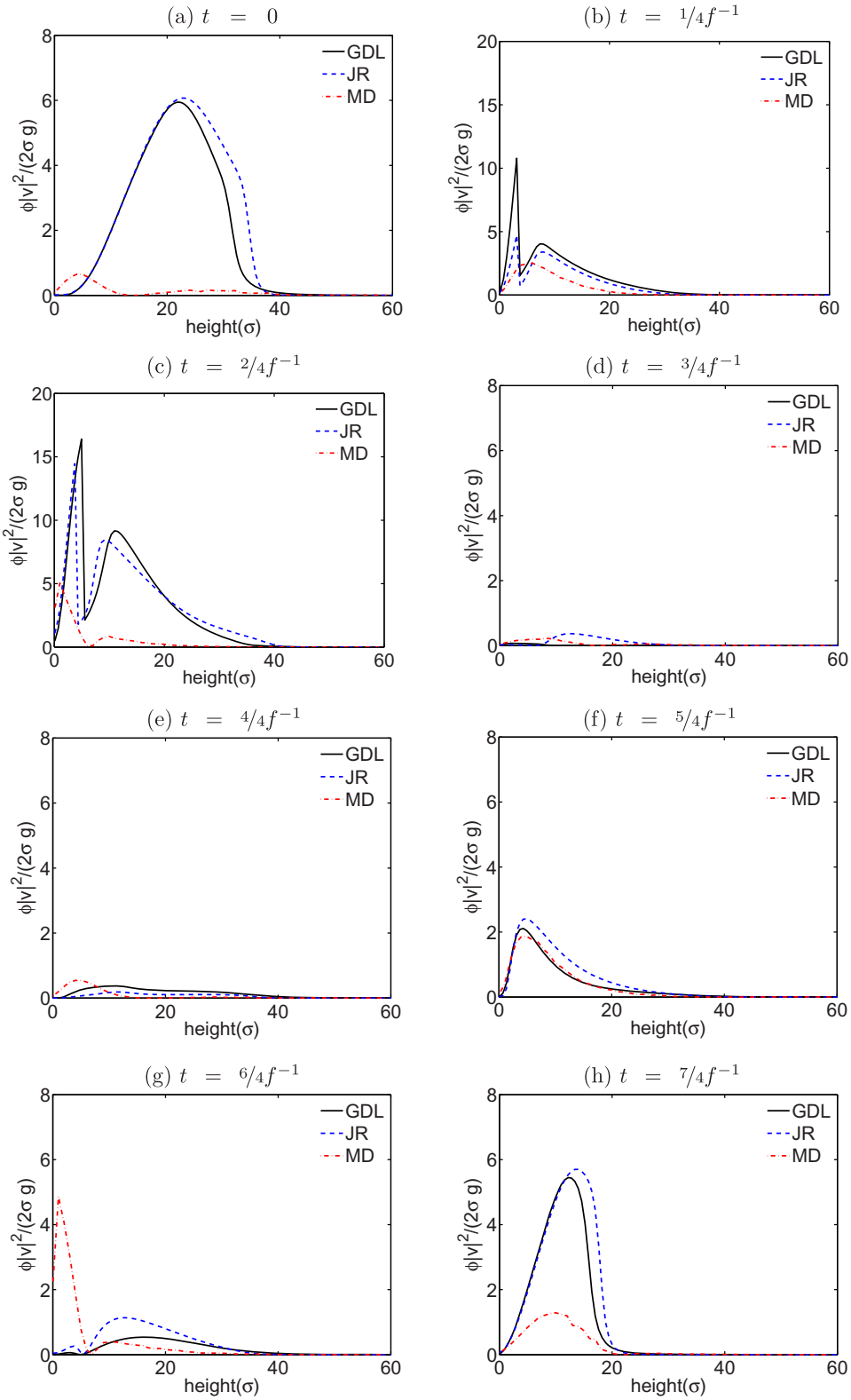

Figure 10. The scaled kinetic energy profiles as a function of height (in units of σ), at selected times over two oscillation periods for the MD, JR and GDL systems. For time evolution of the profiles, see [38].

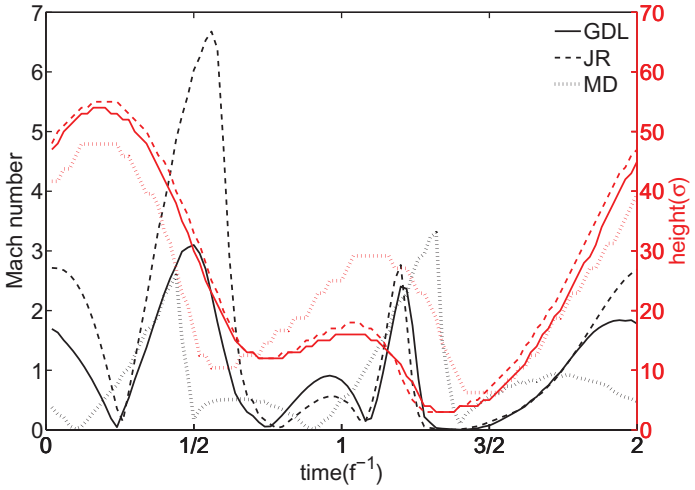

Figure 11. Mach number for the MD system and JR and GDL theories as a function of time, along two periods (f^{-1}) of oscillation of the plate. The red curves indicate the variable height (in diameters) which corresponds to the Mach number shown. These heights are found as the first point in vertical direction from the plate where the packing fraction is 0.1.

with the JR solution. Unlike the JR case, the GDL heat flux consists of two terms, one coming from the temperature gradient, and the other associated, through the coefficient μ, with the density gradient. An analysis of the data reveals that both terms have generally opposite signs. The role of the latter contribution is to transfer heat from the dense toward the dilute regions at the top, while the former brings energy into the granulate, from the high-temperature regions at the top. Both terms are relevant and contribute in the same order of magnitude. So, the heat transfer dynamics is quite different in the GDL and the JR approaches, not only at the top but also at the bottom plate when the impacts occur, in such a way that it gives rise to entirely different solutions for the temperature field.

In general, the GDL system is less diffusive very close to the plate and more at intermediate heights and at the top, as compared with the JR system. The viscosities and the cooling term (see figure 9) also follow this pattern. The analysis of the results allows us to conclude that in the JR system, most of the energy is dissipated very close to the plate, whereas much less is diffused; in the GDL, comparatively, there is less dissipation at the plate and more diffusion.

3.3. Kinetic energy and Mach number

Figure 10 shows the scaled kinetic energy profiles. An examination of the entire sequence shows that the maximum of the kinetic energy is achieved at $t = 0.38\,f^{-1}$ in the GDL simulation, at $t = 0.42\,f^{-1}$ in the JR and at $t = 0.54\,f^{-1}$ in the MD. The GDL peak is the highest, more than four times bigger than the MD and about 50% bigger than the JR. This shows that the GDL solution for the velocity field is also quantitatively different from the JR, a consequence of the inelasticity contributing to the viscosities. Leaving aside the mismatch at the maximum, the JR and GDL solutions go close to each other, and differently from the MD profile, due to the delayed landing of the granular layer in the MD simulation. In any case, the comparison of the kinetic energy profiles reinforces the quite unexpected result that the GDL solution is not closer to the MD, but even further away, than the JR.

Since the GDL temperature is about one order of magnitude higher than JR in the dilute region, the Mach number is also smaller. In figure 11, we can see how the differences are very relevant during stages (c)–(d), when the layer has achieved its maximal extension, and where the JR Mach number is about twice that of the GDL. This is another fact showing that the GDL system is more diffusive than the JR.

The MD curve for the Mach number has been produced using the averaged density and temperature fields in equation (29) for the sound speed, supplied with the equation of state (13).

Unlike JR and GDL approximations, the second MD peak in the Mach number is higher than the first one. Anyway, GDL predicts better the behavior of the Mach number than JR. The values of the Mach number have been computed at the heights shown by the red curves in figure 11. They correspond to the first point, going from the dense to the dilute phase, where the packing fraction is 0.1. There we also find discrepancies when comparing the MD results with those of JR and GDL simulations. This is a consequence of the discrepancies in the density field discussed above.

4. Conclusions

In this paper, we have compared the predictions of the Navier–Stokes hydrodynamic equations of 2D granular gases with MD simulations in a highly nonlinear, far-from-equilibrium problem such as the periodic impact of a horizontal piston which gives rise to the characteristic pattern formation of the Faraday instability. Given that the corresponding Navier–Stokes transport coefficients are not *exactly* known, two different approaches to them have been considered: the JR and GDL approximations. While the first approach applies to nearly elastic particles (in fact, their forms for the transport coefficients are the same as the elastic ones), the latter approximation is much more accurate for granular gases (as verified, for instance, in [23] by comparing the GDL theory with computer simulations at quite extreme values of dissipation) since it incorporates the effect of inelasticity on the transport coefficients. In particular, while the JR theory neglects the term $-\mu\vec{\nabla}n$ in the heat flux, the new transport coefficient μ is clearly different from zero in the GDL theory (see the fourth panel of figure 1). After comparing both approaches with coarse-grained MD results, we can conclude on the following relevant aspects.

First, we conclude that the granular Navier–Stokes hydrodynamics with the proper GDL forms for the transport coefficients η, γ, κ and μ is not capable of reducing the discrepancy between discrete particle simulations and hydrodynamic simulations of moderately dense, inelastic gases. This quantitative disagreement can be due to the fact that while the Navier–Stokes constitutive equations (4) and (5) for the pressure tensor and the heat flux, respectively, apply to first-order in the spatial gradients, the problem analyzed here might be outside the strict validity of the Navier–Stokes approximation as the comparison with MD simulations shows. Surprisingly, the discrepancies between theory and simulations decrease if one considers the elastic forms of the transport coefficients. We think that there are no physical reasons behind this improvement. A similar conclusion has been found in the simple shear flow problem for dilute gases since the non-Newtonian shear viscosity $\eta_s(\alpha)$ to be plugged into the Navier–Stokes hydrodynamic equations is better modeled by the elastic shear viscosity than its corresponding inelastic version $\eta_{GDL}(\alpha)$ (see figure 1 of [32], where while η_s decreases with decreasing α, the opposite happens for η_{GDL}).

Apart from the different α dependence of η, γ and κ, the main difference between the JR and GDL approaches lies in the presence of the coefficient μ in the heat flux. This new transport

coefficient, characteristic of inelastic gases and thus vanishing in the JR theory, constitutes a significant contribution to an enhanced heat transfer mechanism which leads to a high-temperature solution in the dilute region, which is not supported by the particle simulations. Even in the dilute region at the top of the system (figure 1), where shock waves should be completely damped, the GDL model produces an unrealistic energy excess. There, at densities of the order of 0.001 in packing fraction, the coefficient μ is very different from zero.

Thus, we can conclude that the transport coefficient μ is clearly overestimated by the Navier–Stokes approximation and, consequently, the influence of the diffusion term $-\mu\vec{\nabla}n$ on the heat flux is larger than that observed in the simulations. As mentioned before, these discrepancies do not imply that the GDL approach is deficient in any respect. Rather differently, they show the limits of the Navier–Stokes description applied to certain regimes of complex granular flow.

As a matter of fact, in the theory of granular gases, it is well accepted that in certain cases the Navier–Stokes description is insufficient. It was clearly evidenced at the mathematical level, e.g. in [42], that Burnett-order terms are important for the kinetics of granular gases. These terms in the constitutive relations are of second order in the gradients and therefore beyond the Navier–Stokes level of description. In [42], it was shown that these terms are even necessary for a consistent description due to the lack of scale separation in granular gases. The presence of large gradients is quite usual in granular flow, where physical variables may change several orders of magnitude within a distance of a few grains, due to inelastic interactions. That typically manifests in strong shock waves propagating into the system from the boundaries, where the energy source is located. In this way, granular flow is very often supersonic or even hypersonic, and in this regime of extreme gradients the Navier–Stokes description may prove inadequate.

The inclusion of higher-order terms (beyond the Navier–Stokes domain) in the constitutive equations for the momentum and heat fluxes might prove to be a better approximation to problems such as this one, where the first order in the gradients expansion seems insufficient. However, the determination of these nonlinear contributions to the fluxes becomes a very hard task if one starts from the revised Enskog equation. In these cases it is useful to consider kinetic models with the same qualitative features as the Enskog equation but with a mathematically simpler structure [43]. The use of these models allows to derive explicit forms for generalized constitutive equations in complex states driven far from equilibrium, such as the simple shear flow state [44].

In spite of the discrepancies found here, the Navier–Stokes approximation with the GDL forms for the transport coefficients is still appropriate and accurate for a wide class of flows. Some examples include applications of the Navier–Stokes hydrodynamics to symmetry breaking and density/temperature profiles in vibrated gases [26, 27], binary mixtures [45] and supersonic flow past a wedge in real experiments [4, 46, 47]. Another group refers to spatial perturbations of the homogeneous cooling state for an isolated system where the MD results of the critical length for the onset of vortices and clusters [48, 49] are successfully compared with the predictions from linear stability analysis [50] performed on the basis of the GDL transport coefficients.

In summary, the Navier–Stokes theory has shown limitations when exploring the highly nonlinear problem of granular Faraday instability. In particular, the presence of rarefied regions where strong transient shock wave fronts propagate seems to justify the inclusion of higher-order gradients in the transport equations, going beyond the Navier–Stokes approximation [42]. In spite of that, both GDL and JR models work quite well, although here the main discrepancy

is attributed to the term in the heat flux coupled to the density gradient, which is the missing contribution in the JR approach that the inelastic theory comes to fix. More work has to be done in this respect to clarify the conditions under which the Navier–Stokes approximation fails to describe appropriately the granular heat transport. Finally, as a complementary route to the Navier–Stokes approximation, one could numerically solve the Enskog equation via the direct simulation Monte Carlo method [51, 52]. Presumably, the numerical solution would give better quantitative agreement with MD simulations than the Navier–Stokes results reported here. This is quite an interesting problem to be addressed in the future for the Faraday and other different problems such as the simple shear flow or homogeneous states.

Acknowledgments

LA and JAC were partially supported by the project MTM2011-27739-C04-02 DGI (Spain) and 2009-SGR-345 from AGAUR-Generalitat de Catalunya. LA, JAC and CS acknowledge support from the project Ingenio Mathematica FUT-C4-0175. CS and VG acknowledge funding from projects DPI2010-17212 (CS) and FIS2010-16587 (VG) of the Spanish Ministry of Science and Innovation. The latter project (FIS2010-16587) is partially financed by FEDER funds and by the Junta de Extremadura (Spain) through grant number GR10158. LA and TP were supported by Deutsche Forschungsgemeinschaft through the Cluster of Excellence *Engineering of Advanced Materials*. JAC acknowledges support from the Royal Society through a Wolfson Research Merit Award. This work was supported by the Engineering and Physical Sciences Research Council under grant number EP/K008404/1.

References

[1] Jenkins J and Richman M W 1985 *Arch. Ration. Mech. Anal.* **87** 355
[2] Jenkins J and Richman M W 1985 *Phys. Fluids* **28** 3485
[3] Bizon C, Shattuck M D, Swift J B and Swinney H L 1999 *Phys. Rev.* E **60** 4340
[4] Rericha E C, Bizon C, Shattuck M D and Swinney H L 2001 *Phys. Rev. Lett.* **88** 014302
[5] Bougie J, Moon S J, Swift J B and Swinney H L 2002 *Phys. Rev.* E **66** 051301
[6] Bougie J, Kreft J, Swift J B and Swinney H L 2005 *Phys. Rev.* E **71** 021301
[7] Carrillo J A, Pöschel T and Salueña C 2008 *J. Fluid Mech.* **597** 119
[8] Bougie J 2010 *Phys. Rev.* E **81** 032301
[9] Bougie J and Duckert K 2011 *Phys. Rev.* E **83** 011303
[10] Melo F, Umbanhowar P and Swinney H L 1994 *Phys. Rev. Lett.* **72** 172
[11] Melo F, Umbanhowar P B and Swinney H L 1995 *Phys. Rev. Lett.* **75** 3838
[12] Hill S A and Mazenko G F 2003 *Phys. Rev.* E **67** 061302
[13] Brilliantov N V, Salueña C, Schwager T and Pöschel T 2004 *Phys. Rev. Lett.* **93** 134301
[14] Meerson B, Pöschel T and Bromberg Y 2003 *Phys. Rev. Lett.* **91** 024301
[15] Meerson B, Pöschel T, Sasorov P V and Schwager T 2004 *Phys. Rev.* E **69** 021302
[16] Eshuis P, van der Meer D, Alam M, van Gerner H J, van der Weele K and Lohse D 2010 *Phys. Rev. Lett.* **104** 038001
[17] Faraday M 1831 *Phil. Trans. R. Soc.* **121** 299
[18] Garzó V and Dufty J W 1999 *Phys. Rev.* E **59** 5895
[19] Lutsko J F 2005 *Phys. Rev.* E **72** 021306
[20] Chapman S and Cowling T G 1970 *The Mathematical Theory of Nonuniform Gases* (London: Cambridge University Press)

[21] Brey J J and Ruiz-Montero M J 2004 *Phys. Rev.* E **70** 051301
[22] Brey J J, Ruiz-Montero M J, Maynar P and García de Soria I 2005 *J. Phys.: Condens. Matter* **17** S2489
[23] Garzó V, Santos A and Montanero J M 2007 *Physica* A **376** 94
[24] Shu C W 1998 *Advanced Numerical Approximation of Nonlinear Hyperbolic equations* (*Lecture Notes in Mathematics* vol 1697) ed C Cockburn, B Johnson, C W Shu and E Tadmor (Berlin: Springer) p 325
[25] Soto R, Mareschal M and Risso D 1999 *Phys. Rev. Lett.* **83** 5003
[26] Brey J J, Ruiz Montero M J and Moreno F 2001 *Phys. Rev.* E **63** 061305
[27] Brey J J, Ruiz Montero M J, Moreno F and García Rojo R 2002 *Phys. Rev.* E **65** 061302
[28] Goldshtein A and Shapiro M 1995 *J. Fluid Mech.* **282** 75
[29] Brey J J, Dufty J W and Santos A 1997 *J. Stat. Phys.* **87** 1051
[30] Brilliantov N and Pöschel T 2004 *Kinetic Theory of Granular Gases* (Oxford: Oxford University Press)
[31] Goldhirsch I 2003 *Annu. Rev. Fluid Mech.* **35** 267
[32] Santos A, Garzó V and Dufty J W 2004 *Phys. Rev.* E **69** 061303
[33] Grad H 1949 *Commun. Pure Appl. Math.* **2** 331
[34] Gass D M 1970 *J. Chem. Phys.* **54** 1898
[35] Torquato S 1995 *Phys. Rev.* E **51** 3170
[36] Garzó V 2012 arXiv:1204.5114
[37] Jiang G and Shu C W 1996 *J. Comput. Phys.* **126** 202
[38] Almazán L, Carrillo J A, Garzó V, Salueña C and Pöschel T 2012 *Supplementary Online Material* http://msssrv01.mss.uni-erlangen.de/lidia/
[39] van Noije T P C, Ernst M H, Brito R and Orza J A G 1997 *Phys. Rev. Lett* **79** 411
[40] Brey J, Maynar P and Garcia de Soria M I 2009 *Phys. Rev.* E **79** 051305
[41] Costantini G and Puglisi A 2010 *Phys. Rev.* E **82** 011305
[42] Goldhirsch I 2008 *Powder Technol.* **182** 130
[43] Brey J J, Dufty J W and Santos A 1999 *J. Stat. Phys.* **97** 281
[44] Montanero J M, Garzó V, Santos A and Brey J J 1999 *J. Fluid Mech.* **389** 391
[45] Dahl S R, Hrenya C M, Garzó V and Dufty J W 2002 *Phys. Rev.* E **66** 041301
[46] Yang X, Huan C, Candela D, Mair R W and Walsworth R L 2002 *Phys. Rev. Lett.* **88** 044301
[47] Huan C, Yang X, Candela D, Mair R W and Walsworth R L 2004 *Phys. Rev.* E **69** 041302
[48] Mitrano P P, Dahl S R, Cromer D J, Pacella M S and Hrenya C M 2011 *Phys. Fluids* **23** 093303
[49] Mitrano P P, Garzó V, Hilger A H, Ewasko C J and Hrenya C M 2012 *Phys. Rev.* E **85** 041303
[50] Garzó V 2005 *Phys. Rev.* E **72** 021106
[51] Bird G A 1994 *Molecular Gas Dynamics and the Direct Simulation of Gas Flows* (Oxford: Clarendon)
[52] Montanero J M and Santos A 1996 *Phys. Rev.* E **54** 438